International Forum on Aeroelasticity and Structural Dynamics
IFASD 2017
25-28 June 2017 Como, Italy

TOPOLOGY OPTIMISATION OF REPRESENTATIVE AIRCRAFT WING GEOMETRIES WITH AN EXPERIMENTAL VALIDATION

David J. Munk[1], Gareth A. Vio[1], Nicholas F. Giannelis[1], Jonathan E. Cooper[2]

[1]School of Aerospace, Mechanical and Mechatronics Engineering
The University of Sydney, Sydney, NSW 2006 Australia
david.munk@sydney.edu.au
gareth.vio@sydney.edu.au
nicholas.giannelis@sydney.edu.au

[2]Department of Aerospace Engineering
University of Bristol, Bristol BS8 1TH The United Kingdom
j.e.cooper@bristol.ac.uk

Keywords: Topology, optimisation, vibrations, resonance

Abstract: Increasingly aircraft are being designed to be more environmentally friendly and fuel efficient, as defined by the 2020-Vision and Flight-Path EU initiatives. This entails a reduction in aircraft weight while still maintaining all the other constraints. The conventional, semi-monocoque, aircraft design has not changed for the past 50 years. Recently, developments in aircraft design has mainly come from the use of novel materials. A technique has recently been proposed, whereby topology optimisation is used, to determine the material distribution of simple flat plate wings for improved flutter characteristics. It was found that by modifying eigenmode shapes and separating the static natural frequencies the flutter velocity of the simple models could be improved. However, topology optimisation of continuum structures for dynamic stability is, thus far, limited to relatively small design problems. Therefore, this study has two aims. Firstly, it is to extend the method to representative aircraft wing structures and secondly to verify the theoretical results by experiment.

1 INTRODUCTION

Structural topology optimisation strives to find, through material distribution, the optimum for a given objective and constraints, such as a prescribed amount of material [1]. Topology optimisation has evolved dramatically over the past two decades [2]. However, has only been recently applied to aircraft design. One such example is the design of the inboard inner and outer fixed leading edge ribs and fuselage door intercostals of the Airbus A380 aircraft [3]. This application is estimated to have saved 1000kg per A380 aircraft, resulting in reduced fuel burn. Early efforts to apply topology optimisation to aircraft design used truss topology optimisation to design the internal structure for aircraft wings [4]. More recently, the Solid Isotropic Material with Penalisation (SIMP) method has been applied to cut-out design, in pre-defined internal structures [5] and to find optimal internal wing structures, with respect to stiffness, without a predefined internal structure [6,7]. Therefore, topology optimisation has previously been used for improving aircraft wing designs, providing alternatives to the traditional structural layout. However, the full potential of topology optimisation for aircraft design has not been realised, since the objective has primarily been limited to considering strength criteria. Thus, the dynamic criteria of a wing has only be considered as an objective for simple wing models [8,9].

Topology optimisation with respect to eigenfrequencies of structural vibration was first considered by Diaz and Kikuchi [10]. They dealt with single frequency design of plane disks. Subsequently, several studies presented different formulations for simultaneous maximisation of several frequencies for free vibrating plate and disk structures [11–13]. These early studies noticed numerical instabilities that are present in topology optimisation for dynamic stability, such as localised spurious modes and mode switching, which often caused non-convergence of the solution. A technique to avoid these spurious modes was given by Pedersen [14], who dealt with maximum fundamental eigenfrequency design of plates. More recent studies applied a variable bound formulation [15], for the facilitation of multiple eigenfrequencies [16,17]. These studies deal with the maximisation of the separation of adjacent eigenfrequencies for single and bi-material plates. Furthermore, the maximisation of the dynamic stiffness of elastic structures subjected to time-harmonic external loading of given frequency and amplitude have been solved by topology optimisation [18–20]. Similarly, topology optimisation for minimum vibration amplitude response for a given range of excitation frequencies has been performed [21, 22]. For recent papers on minimum frequency response the reader is advised to seek out the work of Yoon [23] and Shu *et al.* [24].

In topology optimisation it is often found that, although an eigenfrequency is simple during the initial stages of the iterative design procedure, at a certain stage it may become multiple due to coincidence with one or more of its adjacent eigenfrequencies [25]. In order to capture this behaviour, a more general solution procedure that allows for multiplicity of the eigenfrequency must be applied. Furthermore, the appearance of artificial modes in low density regions, which occur as very localised modes in regions with relatively large mass to stiffness ratio, become significant in eigenvalue optimisation [26]. For the SIMP interpolation model this occurs as the density goes to zero. To overcome these problems, recently Munk *et al.* proposed a novel moving iso-surface threshold technique [27, 28]. The authors showed that if the element mass-to-stiffness ratio remains finite as density is reduced then the erroneous appearance of localised modes are avoided. Moreover, by ensuring that all modes stay within a pre-defined tolerance from each other one can ensure that the eigenvalues do not become multiple during the entire optimisation. Additionally, for hard-kill methods (where the finite elements are completely removed from the design space), it was recently shown that convergence issues may arise when the sensitivity number of an element varies significantly with respect to its normalised density [29]. Thus a connectivity filter, where the connectivity of the structure is ensured throughout the design process, is implemented to avoid convergence issues.

In aircraft structures the onset of flutter, a dynamic instability characterised by a sustained growth in vibration amplitude, is normally due to the coupling of two neighbouring modes. Traditional methods to eliminate flutter in the aerospace industry usually involve adding extra mass to the leading edge of the wings; solving the problem with the expense of extra weight. If it were possible to design a wing structure that is not based on the traditional model, one might be able to decouple the critical modes for the entire flight envelope. This paper aims to extend the theoretically concepts developed in [8] to structures representative of aircraft wings and to provide an experimental validation for the theoretical results.

2 METHODOLOGY

This study uses the SIMP method for the dynamic stability of structures, through frequency and mode shape manipulation, to maximise the fundamental frequency and separation between neighbouring modes of aircraft wings. SIMP was initially introduced [30] as an easy, but artifi-

cial, way of reducing the complexity of the earlier homogenization approach [1]. Furthermore, improving its convergence to solid-void topologies. However, since then, a physical justification of SIMP has been provided [31] and it has gone on to become one of the most popular techniques for structural topology optimisation [32]. The objective is to separate neighbouring frequencies with a constraint on the fundamental frequency and likeness of mode shapes, determined through the Model Assurance Criteria (MAC) [33]. Therefore, the optimisation problem can be defined by,

$$\begin{array}{ll} \text{Maximise:} & \omega_{n_k} - \omega_{n_l} \\ \text{Subject to:} & \left([\mathbf{K}] - \omega_n^2[\mathbf{M}]\right)\{\Phi_n\} = 0 \\ & \{\Phi_n\}^T[\mathbf{M}]\{\Phi_n\} = 1 \\ & \sum_{i=0}^{i=n} x_i \leq V \\ & \omega_{n_1} \geq \xi \\ & MAC \leq \epsilon \\ & \mathbf{x} = [x_{min}, 1]^n \end{array} \tag{1}$$

where ω_n is the eigenfrequency and Φ_n the corresponding eigenvector, here the subscript k and l specify the modes that are being separated. $[\mathbf{K}]$ and $[\mathbf{M}]$ are the stiffness and mass matrices, respectively. V is volume constraint, or the maximum volume of solid material allowed in the final design, $\mathbf{x}$ is the vector of the design variables, x_i, x_{min} is the minimum value the design variable can take (10^{-3}) and n is the total number of elements in the model. ξ and ϵ are the minimum fundamental frequency, ω_{n_1}, and maximum likeness of the mode shapes, respectively.

In Finite Element Analysis (FEA) the dynamic behaviour of structures is modelled by the eigenvalue problem:

$$\left([\mathbf{K}] - \omega_n^2[\mathbf{M}]\right)\{\Phi_n\} = 0 \tag{2}$$

Therefore, the eigenvalue, ω_n, can be related to the eigenvector, $\{\Phi_n\}$, through the Rayleigh quotient:

$$\frac{\{\Phi_n\}^T[\mathbf{K}]\{\Phi_n\}}{\{\Phi_n\}^T[\mathbf{M}]\{\Phi_n\}} \tag{3}$$

From Eq. 3, the sensitivity of the objective function (Eq. 1) can be calculated by,

$$\begin{array}{ll} \frac{\partial \omega_n}{\partial x_i} = \frac{1}{2\omega_n \{\Phi_n\}^T[\mathbf{M}]\{\Phi_n\}} & \left[2\frac{\partial \{\Phi_n\}^T}{\partial x_i}\left([\mathbf{K}] - \omega_n^2[\mathbf{M}]\right)\{\Phi_n\} + \ldots \right. \\ & \left. \{\Phi_n\}^T\left(\frac{\partial [\mathbf{K}]}{\partial x_i} - \omega_n^2 \frac{\partial [\mathbf{M}]}{\partial x_i}\right)\{\Phi_n\}\right] \end{array} \tag{4}$$

From Eq. 1 it is known that: $\left([\mathbf{K}] - \omega_n^2[\mathbf{M}]\right)\{\Phi_n\} = 0$ and $\{\Phi_n\}^T[\mathbf{M}]\{\Phi_n\} = 1$. Therefore, Eq. 4 can be simplified to:

$$\frac{\partial \omega_n}{\partial x_i} = \frac{1}{2\omega_n}\left[\{\Phi_n\}^T\left(\frac{\partial [\mathbf{K}]}{\partial x_i} - \omega_n^2 \frac{\partial [\mathbf{M}]}{\partial x_i}\right)\{\Phi_n\}\right] \tag{5}$$

Using the material interpolation scheme as given in [27], the derivatives of the mass and stiffness matrices are found by,

$$\frac{\partial[\mathbf{K}]}{\partial x_i} = \frac{1 - x_{min}}{1 - x_{min}^p} p x_i^{p-1} [\mathbf{K}]_0 \tag{6}$$

$$\frac{\partial[\mathbf{M}]}{\partial x_i} = [\mathbf{M}]_0 \tag{7}$$

Here $[\mathbf{K}]_0$ and $[\mathbf{M}]_0$ are the element mass and stiffness matrices for solid elements. Thus, substituting Eqs. 6 and 7 into Eq. 5 gives:

$$\frac{\partial \omega_n}{\partial x_i} = \frac{1}{2\omega_n} \left[\{\Phi_n\}^T \left(\frac{1 - x_{min}}{1 - x_{min}^p} p x_i^{p-1} [\mathbf{K}]_0 - \omega_n^2 [\mathbf{M}]_0 \right) \{\Phi_n\} \right] \tag{8}$$

The sensitivity number (Eq. 8) is an indicator of the change in the eigenvalue, ω_n^2, as a result of the removal of the i^{th} element. Thus, for the separation of two frequencies, k and l, the sensitivity number, α, can be found by,

$$\alpha = \frac{\partial \omega_{n_k}}{\partial x_i} - \frac{\partial \omega_{n_l}}{\partial x_i} \tag{9}$$

Similarly, a sensitivity number must be derived for the mode shape constraint. As already mentioned, the MAC criteria is used to find the likeness of modes, which can be found by:

$$MAC = \frac{\left(\{\Phi_k\}^T \{\Phi_l\} \right)^2}{\left(\{\Phi_k\}^T \{\Phi_k\} \right) \left(\{\Phi_l\}^T \{\Phi_l\} \right)} \tag{10}$$

Therefore, by differentiating Eq. 10 with respect to the design variables, x_i, the sensitivity numbers can be found by,

$$\frac{\partial MAC}{\partial x_i} = \alpha_n^T \frac{\partial[\mathbf{K}]}{\partial x_i} \{\Phi_n\} + \left[a \{\Phi_n\}^T - \omega_n^2 \alpha_n^T \right] \frac{\partial[\mathbf{M}]}{\partial x_i} \{\Phi_n\} \tag{11}$$

where the Lagrange multipliers, a and α_n are unknown scalers given by,

$$a = \left[\frac{\left(\{\Phi_k\}^T \{\Phi_l\} \right)}{\left(\{\Phi_k\}^T \{\Phi_k\} \right) \left(\{\Phi_l\}^T \{\Phi_l\} \right)} \{\Phi_k\}^T - \frac{\left(\{\Phi_k\}^T \{\Phi_l\} \right)^2}{\left(\{\Phi_k\}^T \{\Phi_k\} \right) \left(\{\Phi_l\}^T \{\Phi_l\} \right)} \{\Phi_l\}^T \right] \tag{12}$$

and

$$\alpha_n = -\alpha_p^T [\mathbf{M}] \{\Phi_n\} \cdot \{\Phi_n\} + \alpha_p \tag{13}$$

where α_p is the particular solution. Therefore, using the sensitivity numbers defined in Eqs. 8, 9 and 11 the optimisation problem (Eq. 1) can be solved.

It has been shown that, for eigenfrequency objectives, numerical instabilities can arise during the optimisation procedure (Sect. 1). These numerical instabilities are magnified for non-linear complex large scale structures [2]. To alleviate this issue, Munk *et al.* developed a simple alternative method for topology optimisation with dynamic objectives [34]. They noticed that nominal stress contours could be derived by applying the vibration mode shapes as displacement fields, defined as the dynamic von Mises stress. They showed that the dynamic von Mises stress and frequency sensitivity numbers (Eq. 9) are equivalent for element removal and addition. Therefore, the sensitivity of the objective function (Eq. 1) can be calculated by,

$$\sigma_{vm_d}^2 = \{\Phi_n\}^T [\mathbf{B}]^T [\mathbf{Z}] [\mathbf{B}] \{\Phi_n\} \tag{14}$$

where $[\mathbf{Z}] = [\mathbf{D}]^T [\mathbf{T}] [\mathbf{D}]$, $[\mathbf{D}]$ and $[\mathbf{B}]$ denote the elastic and strain matrices, respectively and $[\mathbf{T}]$ is the coefficient matrix defined by,

$$[\mathbf{T}] = \begin{bmatrix} 1 & -0.5 & 0 \\ -0.5 & 1 & 0 \\ 0 & 0 & 3 \end{bmatrix} \tag{15}$$

Thus, to avoid numerical instabilities, for the representative aircraft wing geometries Eq. 14 is used as the sensitivity function.

3 RESULTS AND DISCUSSION

In this section the results from this study are presented and discussed. First, the simplified plate wing models will be optimised, solving Eq. 1 with and without a constraint on the fundamental frequency. This is followed by an experimental analysis on the optimised wing geometries determining their dynamic characteristics. Finally, the method is applied to a representative wing model, the NASA Common Research Model (CRM), verifying that the method can be extended to large scale design problems.

3.1 Simplified plate wing

A simplified, rectangular, aircraft wing is optimised for maximum frequency separation to improve its dynamic characteristics. The wing model (Fig. 1) has an aspect ratio of 3 with a chord of 20cm and a span of 60cm and is discretised by 40×120 four node plate elements. The wing has a uniform thickness of 1mm and is made from aluminium, having a Young's modulus of $E = 70$GPa, Poisson's ratio of $\nu = 0.3$ and a density of $\rho = 2700$kg/m^3. The boundary conditions of the wing are a locked root chord, creating a cantilever model. The initial model for the simplified plate wing is illustrated in Fig. 1.

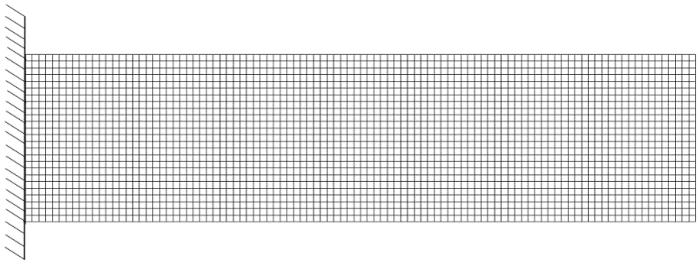

Figure 1: Initial simplified plate wing model.

First the dynamic characteristics of the simplified flat plate wing are determined by running a flutter analysis. From this the flutter speed of the initial wing can be determined, and also the speed at which the wing begins to experience a reduction in damping, and hence, the speed at which the wing will have a reduction in stiffness and begin to oscillate under the dynamic loads.

The corresponding frequency-damping plot for the initial plate wing model (Fig. 1) is shown in Fig. 2.

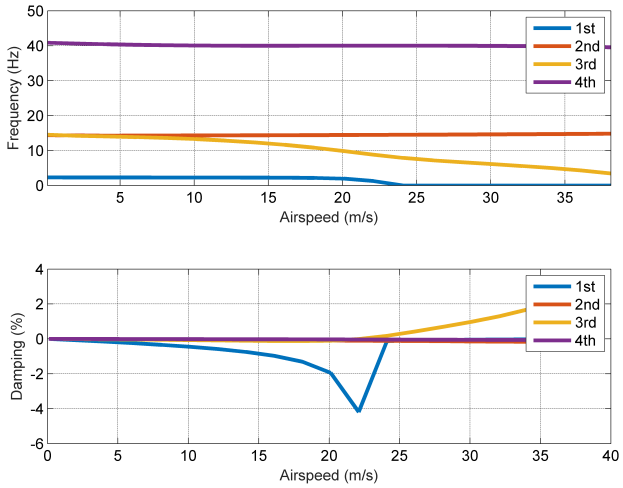

Figure 2: Frequency-damping plot for initial simplified plate wing model.

The first four natural frequencies are plotted, however the first ten were calculated to ensure that the higher energy frequencies are not influential to the dynamic stability of the wing (Fig. 2). As is seen by Fig. 2, at the low speed range, $v = [0, 40]\text{ms}^{-1}$, the first and third natural frequencies undergo significant change, with the third immediately dropping below the second as soon as velocity is applied to the wing. The first natural frequency rapidly drops once a velocity of $v = 20\text{ms}^{-1}$ is reached. For this speed range (Fig. 2), there are two instability modes. The first, is due to the third mode, resulting in a flutter instability at approximately $v = 18\text{ms}^{-1}$. This is seen by the damping ratio of the third mode going from negative to positive damping (Fig. 2). The second, is due to the first mode, resulting in a divergence instability at approximately $v = 23\text{ms}^{-1}$. This is seen by the first mode frequency rapidly declining to zero and the damping ratio converging to zero (Fig. 2). Thus, the model has no stiffness and, as a result, diverges.

The static natural frequencies for the initial model (Fig. 1) can be seen in Fig. 2 by looking at the frequency plot for a velocity of $v = 0\text{ms}^{-1}$. Two main points are observed. First, the second and third natural frequencies are very close, having a natural frequency of $\omega_{n_2} = 14.3822$

and $\omega_{n_3} = 14.5501$Hz, respectively. Second, the fundamental frequency is comparatively low, having a natural frequency of $\omega_{n_1} = 2.3289$Hz. Therefore, the close proximity of the third and second frequencies suggest an instability in one of these modes and the low magnitude of the fundamental frequency promotes divergence. Since, the first instability of the wing is flutter of the third mode (Fig. 2) the separation of the frequencies is more critical to its dynamic stability.

The simplified plate wing is now optimised with the objective of maximum separation between the first ten frequencies (Eq. 1). For this first analysis, the constraint on the fundamental frequency is set to $\xi = 0$Hz, i.e. it is not constrained to give the optimiser complete freedom. Furthermore, to ensure the aspect ratio of the wing is not changed by the optimiser a geometrical constraint is added, defining the border of the plate as non-designable solid material. This technique was also employed in [27]. The wing is optimised for a final volume of 85% of the initial model (Fig. 1), thus reducing the initial mass by 15%. The optimised geometry is given in Fig. 3.

Figure 3: Final design for initial simplified plate wing model without fundamental frequency constraint.

The optimiser has removed material from three zones of the wing (Fig. 3). The largest zone is near the tip of the wing, i.e. the furthest point from the locked boundary condition. This results in a reduction in the second natural frequency, which corresponds to the second bending mode of the wing. Since the wing is still symmetric about the vertical axis, the third mode, which corresponds to the first twisting mode, is practically unchanged. Thus, the optimiser has increased the gap between neighbouring modes by reducing the second and keeping the third constant so that it does not approach the fourth mode. Material is also removed near the root of the wing, where the locked boundary condition is enforced (Fig. 3). This will decrease the first mode, which corresponds to the first bending mode, such that the second mode does not approach the first, avoiding a first and second mode coupling. Therefore, the final design has a minimum frequency separation of $\Delta\omega_n = 8.3626$Hz. However, the fundamental frequency has been reduced by 42% to 1.3567Hz. Therefore, it is expected that the final wing design will be more susceptible to divergence than the initial wing design.

Next, to avoid increasing the wings susceptibility to divergence, a frequency constraint is applied to the optimisation by setting $\xi = \omega_{1_0}$. Where ω_{1_0} is the fundamental frequency of the initial wing design, i.e. 2.3289Hz. Again the wing is optimised for a final volume of 85% of the initial model (Fig. 1). The optimised geometry is given in Fig. 4.

In this case, the optimiser has considerably reduced the amount of material that is removed from near the locked boundary condition. This is to keep the fundamental frequency above the constraint. Furthermore, less material from near the tip has been removed to keep the second fundamental frequency from being decreased down to near the fundamental frequency. Again the wing is symmetric about the vertical axis, hence the frequency of the third mode is almost unchanged. Therefore, the final design has a minimum frequency separation of $\Delta\omega_n = 7.413$Hz. Thus, the minimum frequency separation has been reduced compared to the previous

Figure 4: Final design for initial simplified plate wing model with a fundamental frequency constraint.

optimisation problem, however is still considerably higher than for the initial design ($\Delta\omega_n = 0.1679$Hz). Furthermore, the fundamental frequency has been slightly increased compared to the initial design, from 2.3289Hz to 2.3424Hz. Therefore, this design should not be more susceptible to divergence.

The ability of topology optimisation to design the natural frequencies of simple plate wings has been demonstrated here. The optimiser is able to increase the frequency separation further when there are less physical constraints applied to the problem. However, without the physical constraints the fundamental frequency is significantly reduced, resulting in the promotion of other adverse phenomena, such as stiffness reduction and earlier divergence. The theoretical results from this section will be confirmed experimentally in Sect. 3.2.

3.2 Experiment analysis

The experiments were carried out in the 4×3ft low-speed wind tunnel of the University of Sydney, with a minimum speed of approximately 8.9 m/s and a maximum speed of 60 m/s (clean). The aluminium plates were cut as per the BESO analysis, as shown in Fig. 5. The plates were clamped to the wooden floor of the wind tunnel using a pair of aluminium brackets and steel bolts at zero angle of attack. The wings were decreased with ethanol and a clear plastic stick-on cover was applied over the zones where material was removed, to simulate the wing skin such that the aerodynamic profile remains unchanged. This process was performed on both sides. Marker dots for tracking the wing position were applied. The wing response was recorded using a single high speed SONY RX-100 IV camera, filming at 250 frames per second. It should be noted that only one camera was used, hence any recording would not provide the true displacement, but a projection onto a 2D surface of the 3D displacement.

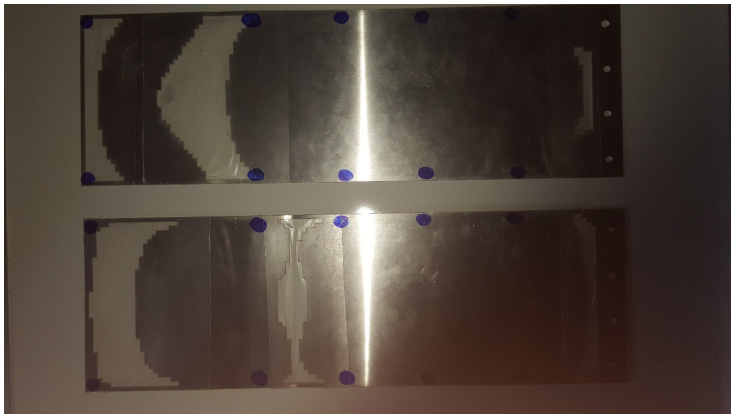

Figure 5: Manufactured wings.

An impulsive test was performed at wind-off condition to check that the equipment was record-

ing and the wing was correctly placed in the field of view, while minimising reflections and it was correctly bolted to the floor brackets. Once the tunnel was started, the speed was slowly increased and recordings of the motion taken. A qualitative indication of the response for both wings is provided in table 1 and 2 at the different airspeeds.

Test speed, ms^{-1}	Qualitative Description of Motion	Test speed, ms^{-1}	Qualitative Description of Motion
00.0	Wind off impulsive test.	13.9	Increase in static deflection.
09.1	Noticeable static deflection.	15.0	Divergence. The wing slowly folded to one side. Fig. 6.
12.1	Some unsteadiness is introduced with buffeting appearing.		

Table 1: Wing without frequency constraint.

(a) (b)

Figure 6: Wing failure without a frequency constraint.

(a) (b)

Figure 7: Wing failure with a frequency constraint.

3.3 Representative wing model

The NASA CRM wing model is optimised for frequency separation to improve its dynamic characteristics. The wing model (Fig. 8) is a full-scale cantilevered wing. The CRM is representative of a modern single-aisle transport aircraft configuration, which was created for collaborative research within the aerodynamics community. It has a wingspan of 58.77m, with an aspect ratio of 9, a taper ratio of 0.275, a leading edge sweep angle of 35° and a break along the trailing edge at 37% of the semi-span. The CRM is discretised by $14 \times 126 \times 3$ eight

Test speed, ms^{-1}	Qualitative Description of Motion	Test speed, ms^{-1}	Qualitative Description of Motion
00.0	Wind off impulsive test.	19.7	High frequency oscillation becomes more prominent with an increase in amplitude (top section of the wing).
11.0	No apparent motion visible, just minor static displacement.	20.4	The oscillation has extended to the whole wing section in a low frequency mode.
15.3	Increase in tip displacement.	20.5	First torsion is becoming apparent with large amplitude oscillation of the trailing edge.
17.0	Some unsteadiness is introduced with buffeting appearing.	20.8	Oscillation growing in amplitude with the trailing edge showing a high frequency response.
17.5	Low frequency flapping motion is introduced.	21.1	Increase in frequency across the whole wing in spanwise and chordwise.
19.0	High frequency oscillation at the tip of the wing.	21.6	Low frequency flap of the whole wing coupling with high frequency of top section of the wing and collapse of the top section as shown in Fig. 7.

Table 2: Wing with frequency constraint.

node solid elements. The CRM is manufactured from aluminium, having a Young's modulus of $E = 70$GPa, Poisson's ratio of $\nu = 0.3$ and a density of $\rho = 2700$kg/m^3. The boundary conditions of the wing are a locked along the entire root chord, to model the cantilever. The initial model for the CRM wing is illustrated in Fig. 8.

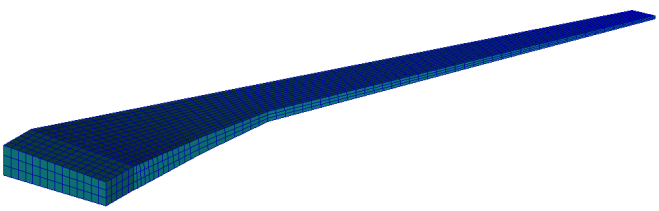

Figure 8: Initial NASA CRM wing model.

A real eigenvalue analysis is performed on the initial CRM wing model to determine its natural frequencies. It is found that the wing model has an initial fundamental frequency of $\omega_{n_1} =$

0.56918Hz and an initial minimum frequency separation, for the first ten modes, of $\Delta\omega_n = 0.7755$Hz. Similarly to the simplified plate wing model, the neighbouring models that have the least separation are the third and second modes. For this analysis, the optimisation problem with a frequency constraint, again defined by $\xi = \omega_{1_0}$, is solved. Where ω_{1_0} is the fundamental frequency of the initial CRM wing design, i.e. 0.56918Hz. The CRM wing is optimised for a final volume of 50% of the initial model (Fig. 8). The optimised internal structure is given in Fig. 9.

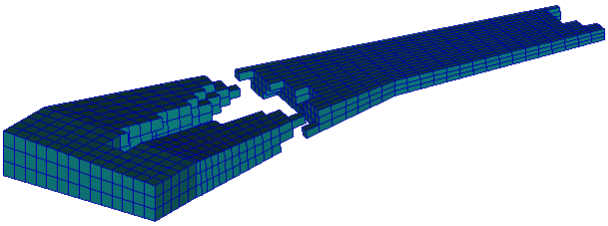

Figure 9: Final design for NASA CRM wing model with a fundamental frequency constraint.

For this analysis the volume constraint is quite low, i.e. the optimiser removes 50% of the initial wing structure. This has resulted in the removal of all the internal structure from the tip section of the wing. This is similar to what was seen in the simple plate wing analysis (Sect. 3.1) and is done to keep the fundamental frequency above the constraint. Furthermore, material has been removed just before the break along the trailing edge. Unlike the simple plate models, in this case the final internal structure is not symmetric about the vertical axis. Therefore, the third mode, which is again the first twisting mode, is increased. However, the initial structure is not symmetric about the vertical axis, unlike the simplified plate wing model, and hence might be why symmetry of the final structure is not observed. The final design has a minimum frequency separation of $\Delta\omega_n = 3.1503$Hz, which is a considerable increase from the initial design of 0.7755Hz. Furthermore, the final fundamental frequency has been increased from 0.56918Hz to 1.3574Hz. However, there are some further points to consider. Namely, no stress or buckling constraints have been implemented, and therefore, the wing is not designed with any strength objectives considered. This is obvious by the large skin panels that have been left without any internal structure. This would definitely result in panel buckling and excess stresses once the aerodynamic load is applied. Therefore, to obtain more realistic internal structure designs these considerations must also be treated by the optimiser.

The ability of topology optimisation to design the natural frequencies of a representative wing model has been demonstrated here. The optimiser is able to increase the frequency separation, whilst also satisfying the physical constraint on the fundamental frequency. Furthermore, no numerical instabilities are present, showing that such methods can be used on large scale problems.

4 CONCLUSION

This work presents a topology optimisation methodology, based on the SIMP method, for the design of the natural frequencies and mode shapes of structures. The method uses the recent dynamic von Mises stress criterion to extend the analysis to representative wing structures. Comparison of the simplified plate model design to low speed wind tunnel experiments show that a constraint on the fundamental frequency is necessary to ensure divergence does not occur,

before the flutter instability. Furthermore, it was shown that the flutter speed could be increased despite the mass being reduced by 15%. This work adds to the current literature on topology optimisation applications to aircraft design and to dynamic objectives in topology optimisation. Finally, it is noted that the current study is solely concerned with dynamic objectives. Especially for the CRM wing model, this results in buckling and stress criteria being exceeded. Therefore, future work is to consider strength objectives along side the dynamic to achieve realisable designs.

5 REFERENCES

[1] Bendsoe, M. (1988). Generating optimal topologies in structural design a homogenization method. *Computer Methods in Applied Mechanics and Engineering*, 71(2), 197–224.

[2] Munk, D. J., Vio, G. A., and Steven, G. P. (2015). Topology and shape optimization methods using evolutionary algorithms: a review. *Structural and Multidisciplinary Optimization*, 52, 613–631.

[3] Krog, L., Tucker, A., Kemp, M., et al. (2004). Topology optimisation of aircraft wing box ribs. In *In: Proceedings of Altair Technology Conference*. Altair Engineering.

[4] Balabanov, V. O. and Haftka, R. T. (1996). Topology optimisation of transport wing internal structure. *Journal of Aircraft*, 33, 232–233.

[5] Stanford, B. and Dunning, P. (2015). Optimal topology of aircraft rib and spar structures under aeroelastic loads. *Journal of Aircraft*, 52, 1298–1311.

[6] Krog, L., Grihon, S., and Marasco, A.-I. (2009). Smart design of structures through topology optimization. In *In: Proceedings of the 8th World Congress on Structural and Multidisciplinary Optimization*. Springer.

[7] Oktay, E., Akay, H., and Sehitoglu, O. (2014). Three-dimensional structural topology optimisation on aerial vehicles under aerodynamic loads. *Computers and Fluids*, 92, 225–232.

[8] Munk, D. J., Vio, A., Gareth, and Cooper, E., Jonathan (2016). Topology optimisation of aircraft structures for flutter supression. In *In: Proceedings of the International Conference on Noise and Vibration Engineering ISMA*. University of Leuven.

[9] Munk, D. J., Boyd, D., and Vio, G. A. (2016). SIMP for complex structures. *Applied Mechanics and Materials*, 846, 535–540.

[10] Diaz, A. R. and Kikuchi, N. (1992). Solutions to shape and topology eigenvalue optimization problems using a homogenization method. *International Journal for Numerical Methods in Engineering*, 35, 1487–1502.

[11] Ma, Z.-D., Cheng, H.-C., and Kikuchi, N. (1994). Structural design for obtaining desired eigenfrequencies by using the topology and shape optimization method. *Computing Systems in Engineering*, 5, 77–89.

[12] Diaz, A. R., Lipton, R., and Soto, C. A. (1994). A new formulation of the problem of optimum reinforcement of Reissner-Mindlin plates. *Computer Methods in Applied Mechanics and Engineering*, 123, 121–139.

[13] Kosaka, I. and Swan, C. C. (1999). A symmetry reduction method for continuum structural topology optimization. *Computers and Structures*, 70, 47–61.

[14] Pedersen, N. L. (2000). Maximization of eigenvalues using topology optimization. *Structural and Multidisciplinary Optimization*, 20, 2–11.

[15] Bendsoe, M. P., Olhoff, N., and Taylor, J. E. (1983). A variational formulation for multicriteria structural optimization. *Journal of Structural Mechanics*, 11, 523–544.

[16] Jensen, J. S. and Pedersen, N. L. (2006). On maximal eigenfrequency separation in two material structures: the 1D and 2D scalar cases. *Journal of Sound and Vibration*, 289, 967–986.

[17] Du, J. and Olhoff, N. (2007). Topological design of freely vibrating continuum structures for maximum values of simple and multiple eigenfrequencies and frequency gaps. *Structural and Multidisciplinary Optimization*, 34, 91–110.

[18] Olhoff, N. and Du, J. (2014). Topological design for minimum dynamic compliance of continuum structures subjected to forced vibration. In *In: Rozvany, G. and Lewinski, T., Eds.* Topology Optimization in Structural and Continuum Mechanics, Int. Center for Mechanical Sciences. Springer.

[19] Kang, Z., Zhang, X., Jiang, S., et al. (2012). On topology optimization of damping layer in shell structures under harmonic excitations. *Structural and Multidisciplinary Optimization*, 46, 51–67.

[20] Yang, X. and Yueming, L. (2013). Topology optimization to minimize the dynamic compliance of a bi-material plate in a thermal environment. *Structural and Multidisciplinary Optimization*, 47, 399–408.

[21] Calvel, S. and Mongeau, M. (2005). Topology optimization of a mechanical component subject to dynamic constraints. Tech. Rep. 05374, LAAS-CNRS.

[22] Jensen, J. S. (2007). Topology optimization of dynamic problems with Pade approximants. *International Journal for Numerical Methods in Engineering*, 72, 1605–1630.

[23] Yoon, G. H. (2010). Structural topology optimization for frequency response problem using model reduction schemes. *Computer Methods in Applied Mechanics and Engineering*, 199, 1744–1763.

[24] Shu, L., Y., W. M., Fang, Z., et al. (2011). Level set based structural topology optimization for minimizing frequency response. *Journal of Sound and Vibration*, 330, 5820–5834.

[25] Rozvany, G. I. N. and Lewinski, T. (2014). *Topology Optimization in Structural and Continuum Mechanics*. New York: Springer.

[26] Bendsoe, M. and Sigmund, O. (2003). *Topology Optimization: Theory, Methods and Applications*. Berlin: Springer.

[27] Munk, D. J., Vio, G. A., and Steven, G. P. (2017). A novel moving iso-surface threshold technique for the vibration optimisation of structures subjected to dynamic loading. *AIAA Journal*, 55, 638–651.

[28] Munk, D. J., Vio, G. A., and Steven, G. P. (2017). A novel method for the vibration optimisation of structures subjected to dynamic loading. *Advances in Aircraft and Spacecraft Science*, 4, 169–184.

[29] Munk, D. J., Vio, G. A., and Steven, G. P. (2017). A bi-directional evolutionary structural optimisation algorithm with an added connectivity constraint. *Finite Elements in Analysis and Design*, 131, 25–42.

[30] Bendsoe, M. (1989). Optimal shape design as a material distribution problem. *Structural Optimization*, 1(4), 193–202.

[31] Bendsoe, M. and Sigmund, O. (1999). Material interpolation schemes in topology optimisation. *Archive of Applied Mechanics*, 69, 635–654.

[32] Rozvany, G. I. N. (2001). Aims, scope, methods, history and unified terminology of computer aided topology optimization in structural mechanics. *Structural and Multidisciplinary Optimization*, 21, 90–108.

[33] Ewins, D. J. (2009). *Modal Testing: Theory, Practice and Application*. New York: Wiley.

[34] Munk, D. J., Vio, G. A., and Steven, G. P. (2017). A simple alternative formulation for structural optimisation with dynamic and buckling objectives. *Structural and Multidisciplinary Optimisation*, 55, 969–986.

COPYRIGHT STATEMENT